Supporting Information

Device Engineering of Chalcogenide Photodiodes with Reduced Dark Current and Enhanced Stability for Underwater Light Communication

*Songxue Bai, Ruiming Li, Xin Chen, Zhenglin Jia, Yong Liu, and Qianqian Lin**

Key Lab of Artificial Micro- and Nano-Structures of Ministry of Education of China, School of Physics and Technology, Wuhan University, Hubei Luojia Laboratory, Wuhan 430072, China

Corresponding Authors

*Email: q.lin@whu.edu.cn

1. Supporting figures
2. Supporting note

1. Supporting figures

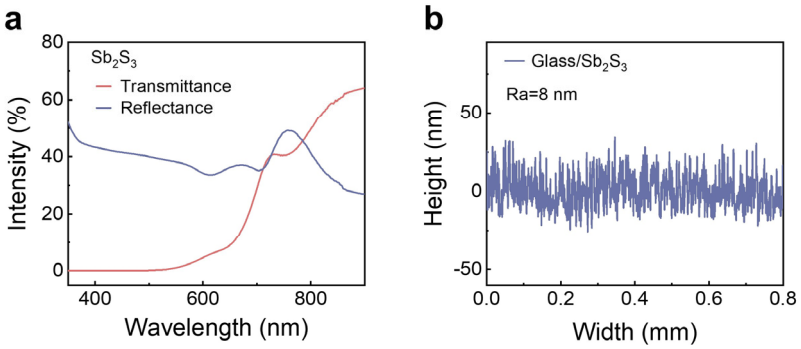

Figure S1. (a) The transmittance and reflectance spectra and (b) surface roughness of Sb_2S_3 thin films annealed at 300ºC.

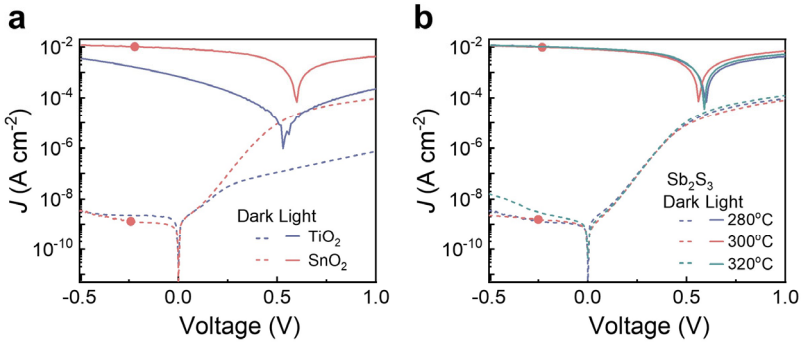

Figure S2. *J-V* curves of Sb_2S_3-based photodiodes fabricated with (a) TiO_2 and SnO_2, and (b) Sb_2S_3 layer with different annealing temperatures.

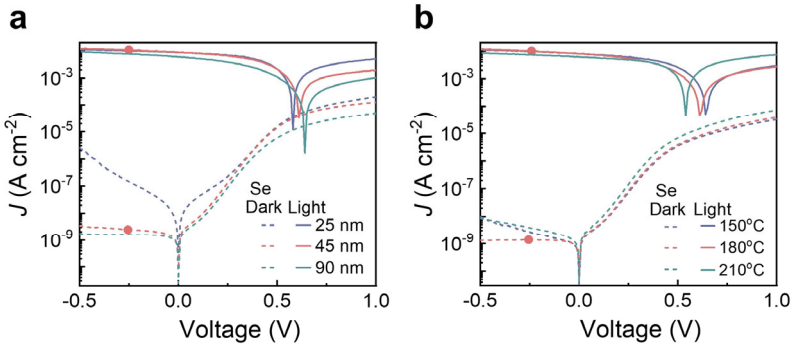

Figure S3. Comparison of *J-V* curves of Sb_2S_3-based photodiodes with different (a) thicknesses and (b) annealing temperatures of Se films.

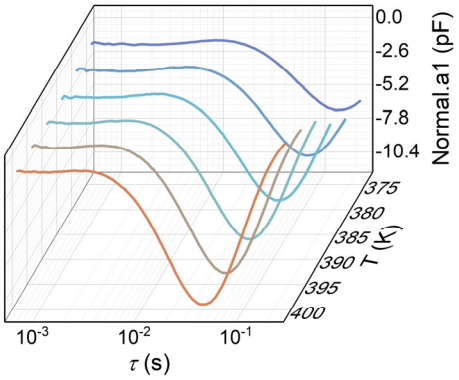

Figure S4. DLTS signals of Sb_2S_3 devices based on Spiro-OMeTAD structure under different temperatures.

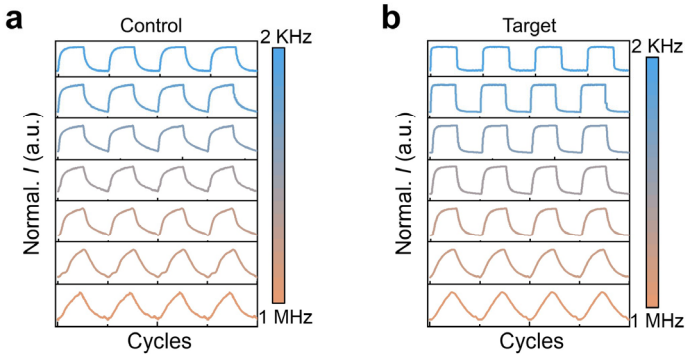

Figure S5. Temporal response of Sb_2S_3-based devices under modulated frequency 530nm LED based on (a) Spiro-OMeTAD and (b) Se/Sb structures.

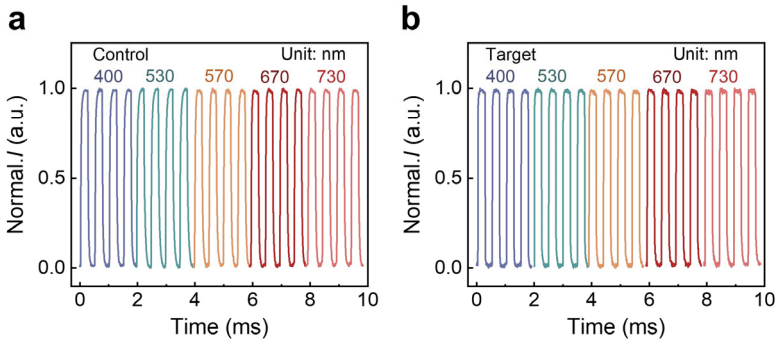

Figure S6. Temporal responses of Sb_2S_3-based devices under various monochromatic LEDs based on (a) Spiro-OMeTAD and (b) Se/Sb structures.

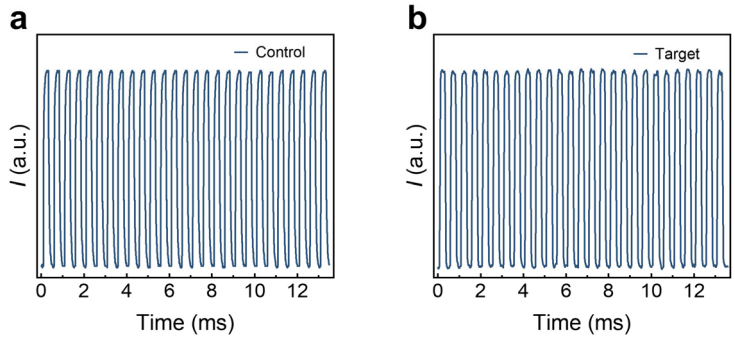

Figure S7. Multiple temporal responses of Sb_2S_3-based devices under modulated 530 nm LED with (a) Spiro-OMeTAD and (b) Se/Sb structures.

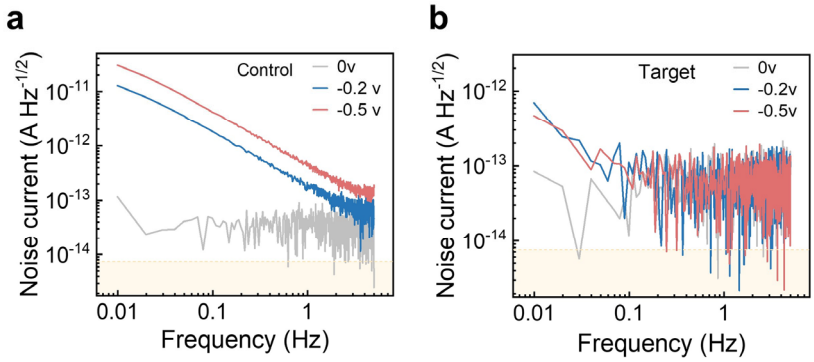

Figure S8. Noise current of the Sb_2S_3-based devices with (a) Spiro-OMeTAD and (b) Se/Sb structures.

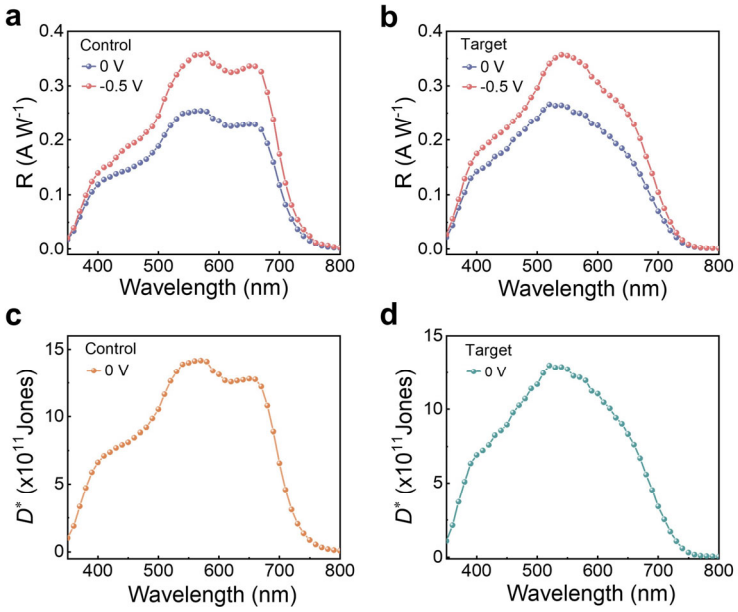

Figure S9. Responsivity of the Sb_2S_3-based devices based on (a) Spiro-OMeTAD and (b) Se/Sb structures. Specific detectivity of the Sb_2S_3-based devices based on (c) Spiro-

OMeTAD and (d) Se/Sb structures.

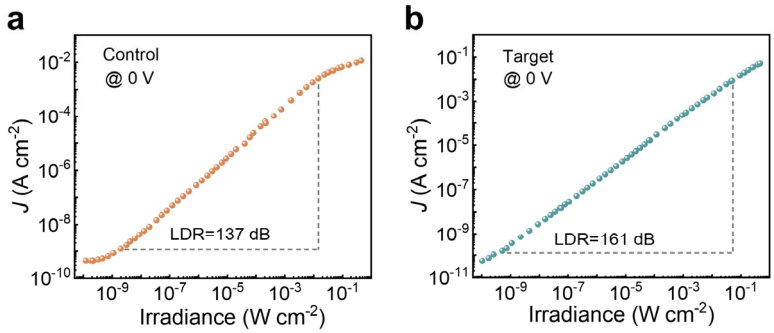

Figure S10. The measured linear dynamic range of Sb_2S_3-based devices based on (a) Spiro-OMeTAD and (b) Se/Sb structures.

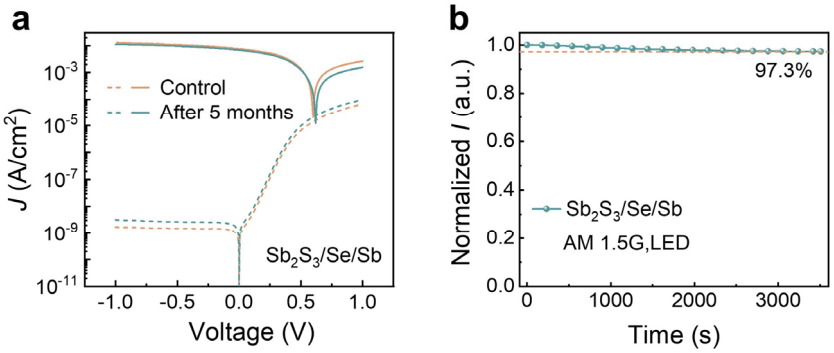

Figure S11. (a) *J-V* curves of the Sb_2S_3/Se/Sb devices illuminated under 1 sun after storing 5 months in an N_2-filled glovebox, (b) normalized transient current tracking of an unencapsulated Sb_2S_3/Se/Sb devices for 1 h in air.

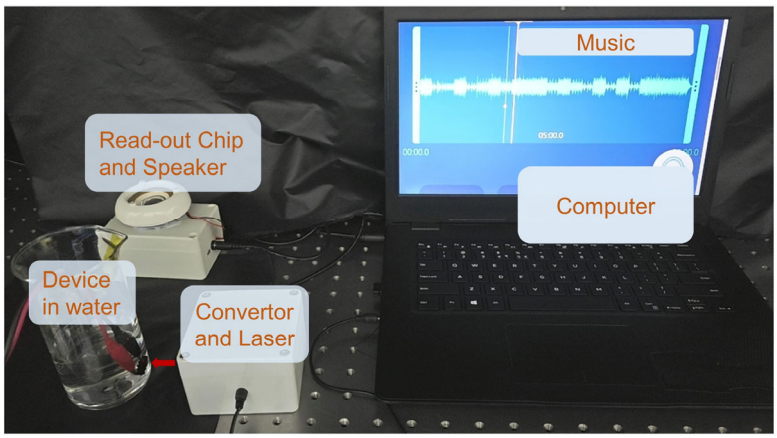

Figure S12. The optical photo of the optical communication test system.

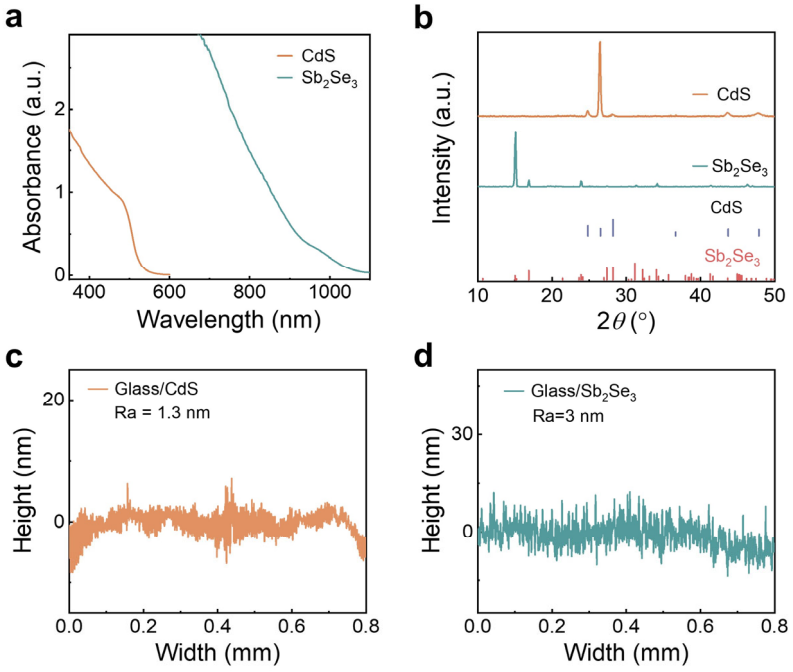

Figure S13. (a) The absorption spectra and (b) the XRD patterns of CdS and Sb_2Se_3 films. The surface roughness of (c) CdS and (d)Sb_2Se_3 films.

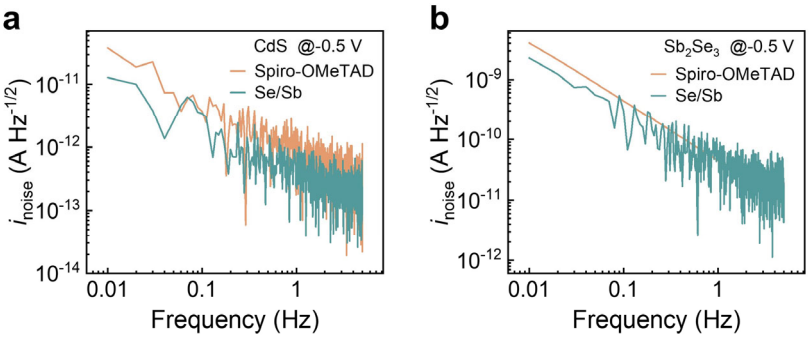

Figure S14. Noise current spectra of (a) CdS-based and (b) Sb_2Se_3-based devices based on Spiro-OMeTAD and Se/Sb structures.

2. Supporting note

Supplementary note 1. Principle of DLTS measurement

There are four main behaviors of deep-level defects in semiconductor materials, namely: trapping electrons (c_e), trapping holes (c_h), emitting electrons (e_e), and emitting holes (e_h). For a general Schottky junction or n^+p (p^+n) junction structure, under the action of negative bias voltage, the majority in SCR is fully depleted, and the depletion region mainly falls in the p(n) region where the carrier concentration is lesser. Therefore, for minority carrier defects with energy levels higher than the Fermi level (E_F) in the depletion region, ideally, they can be regarded as vacancies. Conversely, the majority of defects below the E_F can be considered to be fully occupied. When a positive pulsed voltage is applied to the device, the majority on both sides are rapidly injected into the depletion region and are captured by the deep-level defects. When the positive signal is large enough, the carriers can drift across SCR and fill the minority carrier defects. When the pulse voltage is withdrawn, these deep-level defects re-emit the trapped charges, which is reflected in the transient capacitance change of the device. The emission behavior of a defect at a certain temperature is related to its energy level depth, trapping cross-section, and defect concentration. The specific mathematical expression can consider the situation that the defect state is occupied by carriers, which is expressed as,

$$n_T(t) = \left(N_T - e_p \tau N_T\right) \exp\left(-\frac{t}{\tau}\right) + n_T(\infty), \quad \text{(S1)}$$

where e_p, τ and N_T are emission rate, emission time constant and trap density. Therefore, it can be considered that the transient change of capacitance in this process can also be described by a single exponential function. Also, it can be seen that for the majority and the minority defects, their contribution to the transient capacitance ΔC of the device during the charge emission process is just the opposite while their density can be expressed as ,

$$N_T = \frac{2\Delta C}{C_0} N_D, \quad \text{(S2)}$$

where N_D is the total doping density obtained from C-V measurement and C_0, ΔC are

steady capacitance under reverse bias and amplitude of transient capacitance, respectively. Further, through temperature scanning, the emission behavior of different defects can be extracted separately. Represented by electrons, its emission behavior can be expressed as,

$$e_n(t_1, t_2) = \frac{1}{\tau} = \sigma_n v_{th} N_c \exp\left(-\frac{E_c - E_T}{kT}\right) \propto T^2 \exp\left(-\frac{E_c - E_T}{kT}\right), \quad \text{(S3)}$$

where v_{th}, N_c, E_c, and E_T are thermal velocities, conduction band state density, conduction band depth, and the defect energy level, respectively. In real measurement, τ can be obtained from the maximum value of the DLTS signal using different correlation functions. Therefore, the E_T of the defect can be obtained by constructing the Arrhenius plot.